Analysis of Cord Stress During Tire Dynamic Longitudinal Slip

Shuiting Zhou
Xiamen University of Technology

Luwen Chen (✉ 1210271096@qq.com)
Xiamen University of Technology

Pengfei Sun
Xiamen University of Technology

Junling Meng
Xiamen University of Technology

Chao Qian
Xiamen University of Technology

Xin Sun
Xiamen University of Technology

Research Article

ORIGINAL ARTICLE(or REVIEW)

Analysis of Cord Stress During Tire Dynamic Longitudinal Slip

Shui-Ting Zhou[1, 2]**• Lu-Wen Chen**[1, 2] **• Peng-Fei Sun**[1,2] **• Junling Meng**[1, 2] **• Chao Qian**[1, 2] **• Xin Sun**[1, 2]

Abstract: Select 215/55 R17 radial tires for material test to obtain relevant material parameters. Use these parameters to build a finite element model and conduct longitudinal slip simulation. The relationship between longitudinal force and slip rate at different speeds and loads was determined by tire longitudinal slip tests. Then the longitudinal slip simulation results are compared with the test results to verify the feasibility of the model. The circumferential and axial Rebarforce of the belt layer at different speeds and the extreme value of the circumferential Rebarforce on the reverse-envelope of different skeleton materials are analyzed. The results show that: in the static state, the cord force of the belt layer will show a trend consistent with the direction of the cord arrangement. As the speed increases, the belt cord force exhibits significant fluctuations and asymmetry. The Rebarforce of the turn-up points on the belt and ply is significantly smaller compared to the fetal crown ply. The Rebarforce at the fetal crown and belt wrapping points at 60km/h is smaller than at 40km/h and 80km/h. The cord force of the fetal crown ply and the belt ply is much more affected by the load than that of the ply.

Keywords: Radial tire • Finite element method • Tire cord • Slip ratio

1 Introduction

The tire is the intermediate medium connecting the ground and the car. During the longitudinal skid, the tires mainly play the functions of regulating the speed of the vehicle

✉ Lu-Wen Chen
  1210271096@qq.com

1 School of Mechanical and Automotive Engineering, Xiamen University of Technology, Xiamen 361024, China

2 Fujian Provincial Key Laboratory of Advanced Design and Manufacturing for Passenger Cars, Xiamen 361024, China

and controlling the driving and braking of the vehicle. However, during the longitudinal sliding process, the overall deformation of the tire is severe, and the skeleton material of the tire is prone to damage. Wei Yintao and Shen Xiaoliang [1] predicted the six-component force of the tire by analyzing the steady-state rolling state of the tire. Li Li et al. [2] and Ge Shuqing et al. [3] analyzed the ground contact characteristics and static stiffness of tires through Abaqus software and experiments. Chen Wenyuan et al. [4] analyzed the tire footprint by finite element method. Shoop S et al. [5] studied the motion state and force analysis of radial tires on a deformable base. Jenog KM et al. [6] used finite element technique to study the puncture pressure of the load meridian. Li, Quantong et al. [7] predicted and analyzed the longitudinal slip rate in potholes. Haichao Zhou et al. [8] proposed an estimation method for the longitudinal force of smart tires based on the strain physical model. Zhou et al. [9] studied the static steering mechanics of tires by offsetting the steering axis. Tian et al. [10] and Sun et al. [11] studied the stress and deformation of the cord under high-speed tire conditions and the viscoelasticity of the cord of the dynamic tire, respectively. The above scholars have all conducted a certain analysis on the deformation of the tire under different working conditions and the stress on the cord, but have not conducted a deeper study on the stress on the cord during the longitudinal sliding process of the tire. In this paper, through the combination of experiment and simulation, the deformation and stress of the tire cord under different slip rates are studied. The vulnerable position of tire cord is predicted, and certain enhancement measures are given.

2 Longitudinal Slip Test Theory and Principle

The tire longitudinal slip test is a branch of the tire six-component force test, which mainly studies the relationship between the tire slip rate SR and the longitudinal force Fx at different speeds. As shown in Figure 1, during longitudinal sliding, the longitudinal force Fx is the force acting on the tire along the X-axis by the road. The specific role of tire longitudinal force in the process of driving and braking is to accelerate or decelerate the vehicle. When Fx is positive, the tire is driven. At this time, Fx is the driving force. When Fx is negative, the tire is under braking. At this time, Fx is the braking force. The tire slip rate SR is caused by the difference between the wheel center angular velocity ω_0 and the original wheel center angular velocity ω caused by the deformation of the tire. The specific relationship is as follows:

$$SR = (\omega - \omega_0) / \omega_0 , \qquad (1)$$
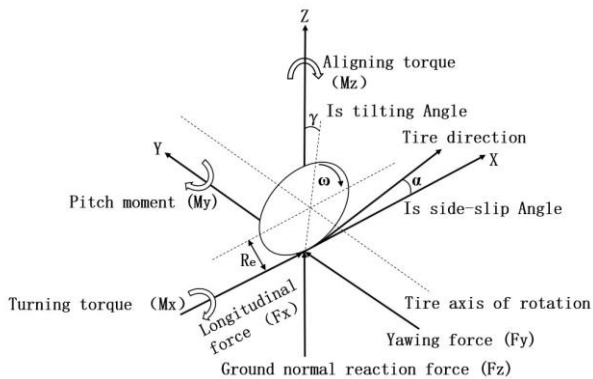

Figure 1 Tire coordinate system

When running a tire slip test, precise control of the speed is required. As shown in Figure 2, the tire is placed on a steel belt supported by two rotating drums. Slip is achieved by applying a fixed angular velocity ω to the tire and simultaneously applying an angular velocity ω_0 to the drum relative to the center of the tire.
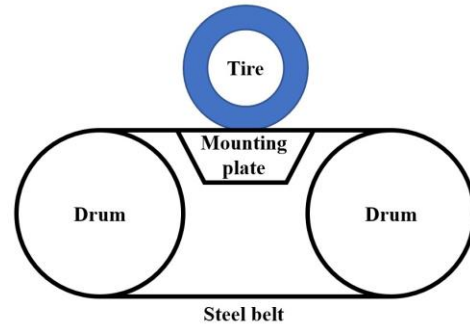

Figure 2 Schematic diagram of steel belt road

The data of the tire test process is measured by sensors on the support platform. The data of driving and braking slip ratios are obtained and then fitted by the PAC2002 model. Its related parameters are shown in Figure 3. The basic form of the PAC2002 tire model formula:

$$y(x) = D\sin[C\arctan\{Bx - E(Bx - \arctan(Bx))\}] , \quad (2)$$

$$Y(x) = y(x) + S_y , \qquad (3)$$

$$x = X + S_h , \qquad (4)$$

where x is the input value, $Y(x)$ is the output value, S_h is the horizontal drift of the curve, S_y is the vertical drift of the curve, and D, C, B and E in the formula are different parameters in the PAC2002 model:

D determines the peak value of the model curve, called the crest factor.

C determines the use of the sine part, so it affects the shape of the overall curve, called the shape factor.

B determines the trend of the extension curve, which is called the stiffness factor.

E corrects the characteristic of the curve near the peak, called the shape factor.
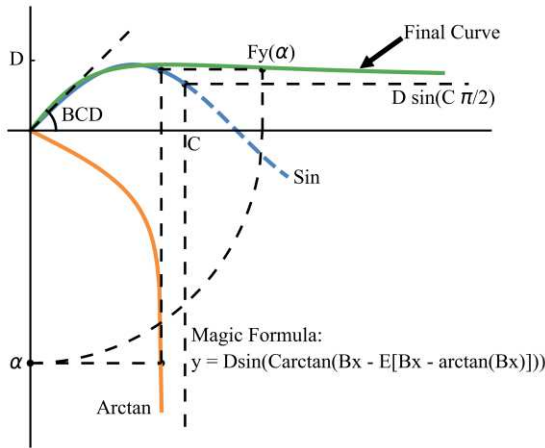
Figure 3 PAC2002 tire model curve and its main influencing parameters

The longitudinal force calculation under pure longitudinal slip condition can be derived from equation (2). In pure longitudinal slip conditions, there is no slip angle. The inputs to the calculation formula are slip rate, vertical load, and roll angle. The output of the formula is the longitudinal force. As shown in formula (5):

$$F_x = F_{x0}(\kappa, F_z, \gamma) \,, \tag{5}$$

$$F_{x0} = D_x \sin\{[C_x \arctan(B_x \kappa_x - E_x(B_x \kappa_x - \arctan(B_x \kappa_x)))]\} + S_{Vx} \,, \tag{6}$$

$$\kappa_x = \kappa + S_{Hx} \,, \tag{7}$$

$$\gamma_x = \gamma \lambda_{\gamma x} \,, \tag{8}$$

where S_{Hx} is the longitudinal drift coefficient, and $\lambda_{\gamma x}$ is the scaling coefficient. In formula (6), Dx, Cx, Bx, Ex, κx, γ_x are first-level parameters, and these first-level parameters can be represented by second-level parameters, third-level parameters, scaling coefficients and standardized increments.

3 Tire Finite Element Model

3.1 Tire Material Test

As shown in Figure 4, the rubber material of each part of the tire and the extracted cord material are placed on a material stretching machine for tensile test. The rubber material is stretched to 3 times its original length, and the skeleton material such as the cord is stretched until it just breaks. The stress-strain parameters of rubber and cord materials were obtained through uniaxial tensile tests of multiple groups of materials.

Figure 4 Material Uniaxial Tensile Testing

Draw the corresponding stress-strain curve from the measured data. The data of tensile and compression tests and several sets of constitutive model data were fitted by Origin software. As shown in Figure 5, the black dotted line is the test data. Blue square lines Mooney-Rivlin constitutive model. The red circle line is the Neo-Hooke constitutive model. The green triangular line is the Yeoh constitutive model. By comparing the test data with the constitutive model, it is found that the tensile data of this tire sample fits the Yeoh model best. Therefore, the relevant fitting formula of Yeoh model is used to perform parameter transformation operation on the original rubber stress-strain curve. Three model parameters of C10, C20, and C30 were obtained, as shown in Table 1. And the corresponding framework material parameters, as shown in Table 2.
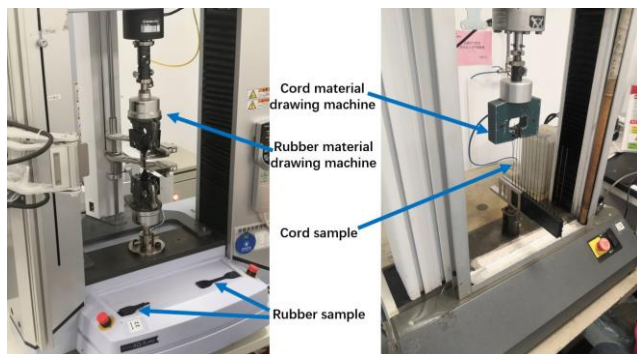
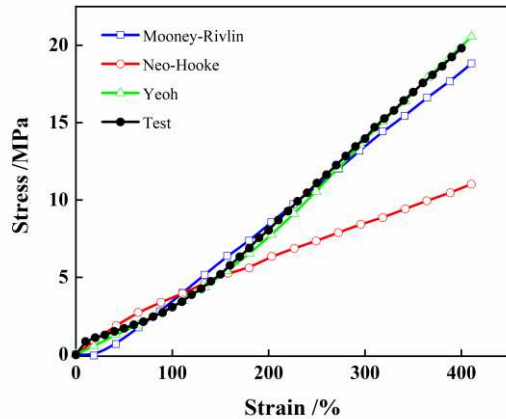**Figure 5**   Constitutive model fitting curve

Table. 1. Yeoh model parameters of different rubber materials

| Rubber type	C_{10}	C_{20}	C_{30}
Tread	0.669470	0.036176	-0.000420
Sidewall	0.382588	0.014033	-0.000091
Apex	2.965836	-0.164619	0.010994
Inner liner	0.495442	0.000405	0.00001
Bead filler	1.061872	0.060687	-0.000922
Wing	0.66047	0.036176	-0.00042
Belt layer	1.602325	0.063284	-0.001573
Ply	0.87901	0.054067	-0.001014
Bead	1.626822	0.1774	-0.009939
Fetal crown layer	0.857678	0.040701	-0.000274

Table. 2. Yeoh model parameters of different rubber materials

| Skeleton material	Young's modulus （MPa）	Poisson's ratio	Bundle diameter （mm）	Arrangement density （Kg·mm⁻³）	Included angle with tyre meridian （°）
1# Belt layer	210729.3	0.29	0.332	1.333	67
2# Belt layer	210729.3	0.29	0.332	1.333	-67
1# Fetal crown layer	5098.8	0.29	0.237	0.909	90
1# Ply	5395.08	0.29	0.237	1	0
2# Ply	5395.08	0.29	0.237	1	0
Bead wire	164498.8	0.29	0.708	1.052	90

3.2   3D Tire Model Establishment

The tire is roughly divided into tread, belt layer, inner liner, bead ring, sidewall, apex and other parts through the above material test. Use Abaqus software to divide the tire section into corresponding Sets and assign corresponding material properties. The tire section is shown in Figure 6(a). The section is then mirrored and processed with the *SYMMETRIC MODEL GENERATION command. Rotate it 360° in the circumferential direction to become a complete pneumatic tire model. The complete 3D tire model is shown in Figure 6(b). The 2D model has 764 nodes and 670 mesh elements. The 3D model has 38,200 nodes and 33,500 mesh elements. The first belt layer is at 67° to the meridian. The second belt layer is at -67° to the meridian direction. The fetal crown layer is 90° to the meridian direction. The first and second plies are both at 0° to the meridian direction.
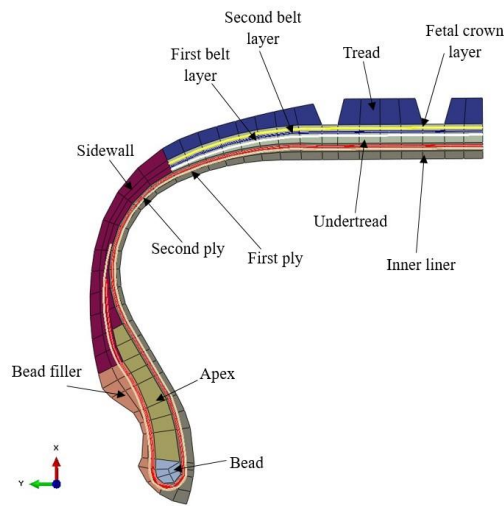
(a) 2337 N
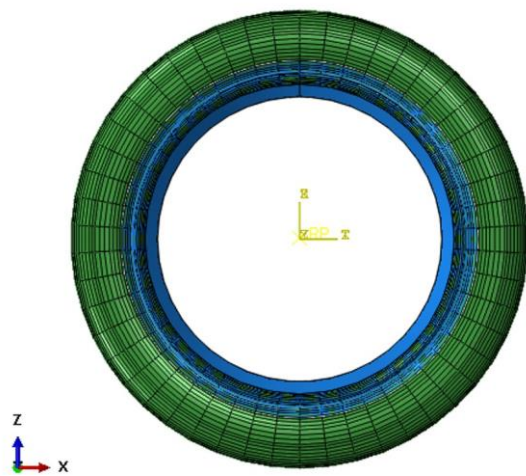
(b) 3936 N

Figure 5   Tire Finite Element Model

4   Tire Longitudinal Slip Test and Longitudinal Force Analysis

4.1   Tire Slip Test

The tire slip test is part of the tire six-component force test. The tire speed and slip rate of the tire are controlled by a six-component force bench test instrument. The longitudinal force is then monitored by the force sensor. As shown in Figure 7, 215/55 R17 radial tires were selected for the test. First, the side slip angle of the tire is controlled to be kept at 0° by the side slip angle controller shown at 2 in Figure 7. Then, the roll angle of the tire is controlled to be kept at 0° by the roll angle controller shown at 3 in Figure 7. Place the tire on the test bench spindle. A fixed rotational speed ω is given, and radial force is applied through the hydraulic rod. The tire is brought into contact with the steel belt shown at 1 in Figure 7. The angular

velocity ω_0 of the steel belt relative to the center of the hub is provided by two large drums. The purpose is to cause a difference in rotational speed with the tire, which will cause it to slip.
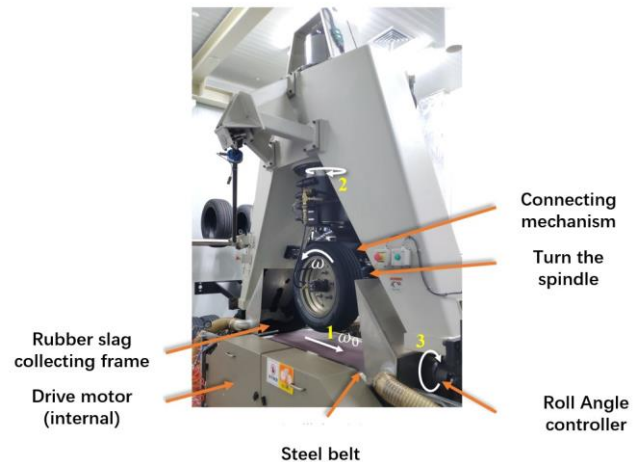

Figure 7   Tire six-component force bench test instrument

4.2   Tire Longitudinal Slip Simulation

Tire longitudinal slip simulation is a finite element analysis that simulates the longitudinal slip test conditions. The main purpose is to study the stress of tire carcass ply and belt layer through computer calculation. Study the area where the tire cord is concentrated during braking and driving, and increase the strength of that location.

The boundary conditions of the tire longitudinal slip simulation are carried out strictly according to the test procedure shown in Figure 7. The longitudinal sliding simulation is shown in Figure 8, and the simulation uses the analytical rigid plate to simulate the ground. The simulation process is divided into four analysis steps: inflation, loading, rotation, and slip. The tire is rotated by applying a fixed angular velocity ω to the center reference point A of the rim. Then, a velocity gradient of an equidistant amplitude curve is applied to the ground reference point B. Make the slip ratio with the tire just between -30 and 30, and complete the entire slip process in one go.
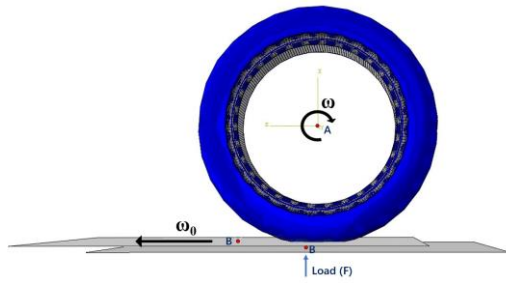
Figure 8   Tire Slip Simulation

The tire test and simulation were kept at 250 kpa tire pressure. As shown in Table 3, the tires were tested and simulated under the working conditions of speeds of 40km/h, 60km/h, 80km/h and loads of 2337N, 3936N, 4920N, and 6396N.

Table. 3. Longitudinal sliding test parameters without roll angle

and yaw angle

Tire pressur（kpa）	Slip ratio（％）	Test speed(km/h)	Vertical load（N）
250	-30～30	40；60；80	2337；3936；4920；6396

4.3   Tire Longitudinal Force Analysis and Model Verification

Through the longitudinal slip test, the relationship between the slip rate and the longitudinal force of the tire under different speeds and load conditions was obtained. Then, the data are fitted by the PAC2002 model-related formulas such as formula (5-8). The slip rate-longitudinal force curve relationship shown in Figure 9 is obtained. It can be seen from Figure 9 (a, b, c) that the tire longitudinal force will increase with the increase of the vertical load, and the change of speed has little effect on the tire longitudinal force. When the slip rate is -30% and 30%, the longitudinal force corresponding to the speed of 60km/h is slightly lower. This shows that under the same slip rate, the longitudinal force of the tire will increase with the increase of speed and decrease with the increase of speed. In the figure, the negative slip rate is the tire braking phase, and the positive slip rate is the tire driving phase. By comparing the positive and negative slippage in the three figures, it is found that the peak longitudinal force of the tire during driving is greater than the peak longitudinal force during braking. This shows that the tire has a greater impact on the handling stability during the driving phase.
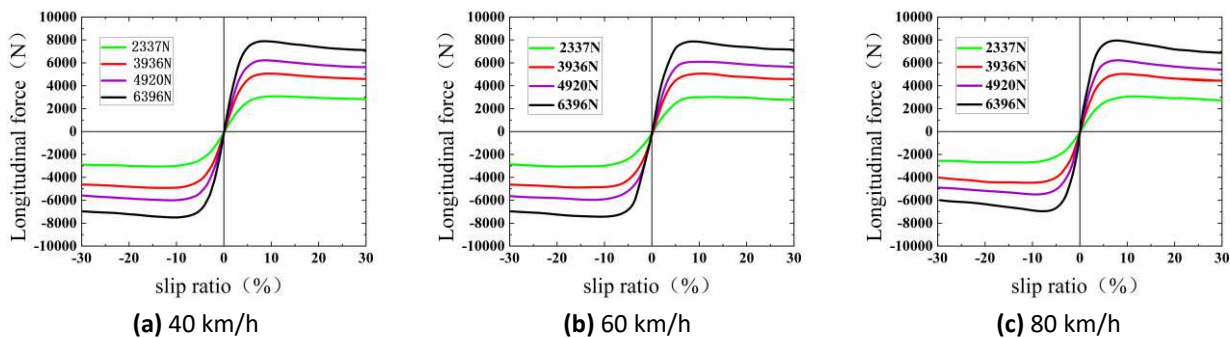

(a) 40 km/h   **(b)** 60 km/h   **(c)** 80 km/h

Figure 9   Slip rate-longitudinal force relationship affected by vertical load at different speeds

Through the analysis of Figure 9, it is found that the longitudinal force of the tire is positively correlated with the vertical load on the tire. It shows that the larger the load, the larger the error of the longitudinal force will be. Therefore, it is only necessary to compare the slip ratio-longitudinal force relationship corresponding to 6396 N at different speeds. As shown in Figure 10, the black curve is the experimental data after fitting, and the blue curve is the simulation data after noise reduction. Measure the maximum offset and calculate it. It is found that the error between the test and the simulation is within 10%, and the simulation can reflect the test process.
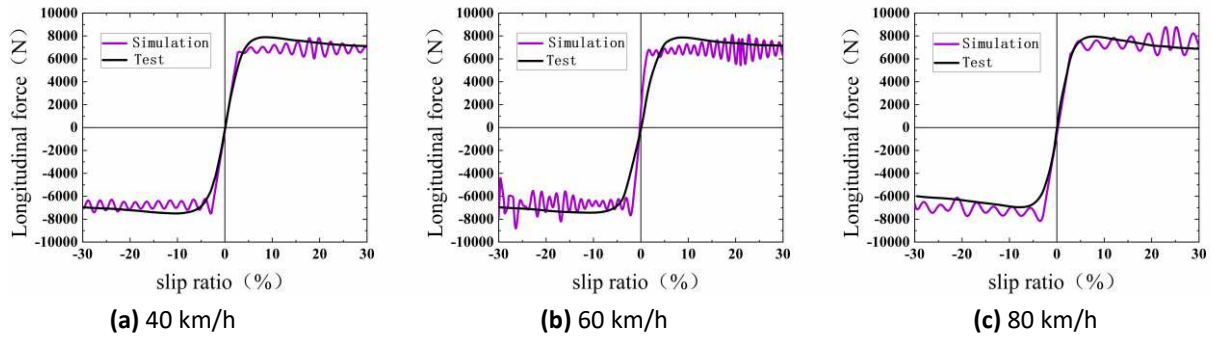
(a) 40 km/h   (b) 60 km/h   (c) 80 km/h

Figure 10   Comparison of Slip Rate-Longitudinal Force Relationship between Simulation and Test at Different Speeds

5   Analysis of Tire Frame Material

The tire carcass colloid and the cord and other skeleton materials are formed by mutual bonding, which causes the turn-up point of the skeleton layer such as the ply to easily cause the rubber to open and separate. This results in tire bulging and plastic deformation [12]. By simulating the longitudinal sliding process of the tire, the force analysis of the fetal crown ply, 1# belt ply and 1# ply in the tire frame material is carried out. As shown in Figure 11, the circumferential Rebarforce analysis is performed on the turn-up points of the three tire frame materials A, B, and C on the tire section. The belt layer is subjected to both circumferential Rebarforce analysis and axial Rebarforce analysis. The schematic diagram of the circumferential and axial directions of the belt layer is shown in Figure 12.
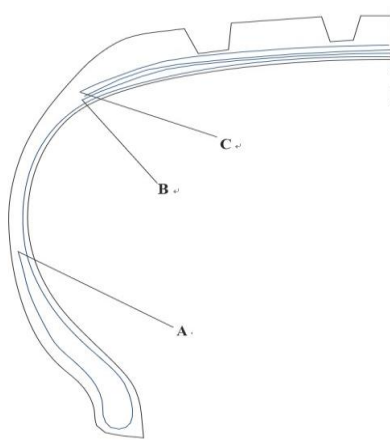

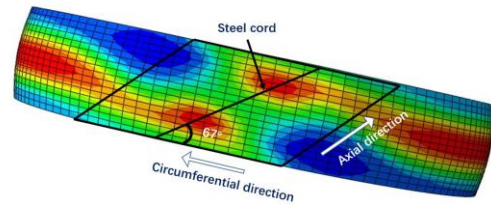**Figure 11**   Analysis points of the cord along the tire circumference

Figure 12   Schematic diagram of belt cord direction

5.1   Axial Force and Asymmetry of Belt Layer

In order to observe the stress condition more clearly, the stress of the cord with a load of 6396N is selected for analysis. The Rebarforce of the tire's first belt ply cord is monitored by finite element. The stress conditions of the belt cord in the tire circumferential and axial directions at 0 km/h, 40 km/h, 60 km/h, and 80 km/h are plotted as shown in Figure 13. Analysis of Figure 13(a) shows that the belt layer exhibits a certain angle of Rebarforce distribution at the grounding position. Comparing with Figure 12, it can be seen that the angle of cord arrangement is consistent with that of the belt layer, which shows that the belt layer has obvious asymmetric phenomenon. At the same time, the stress area of the belt layer is mainly concentrated in the vicinity of 180° in the circumferential direction and 35mm and 140mm in the axial direction. Because this is the shoulder corner of the tire contact area, there will be significant stress changes. Analysis of Figure 13 (b, c, d) shows that the belt cords show obvious fluctuations with the increase of speed. At the same time, the stress concentration point of the belt layer will also spread from the contact center to various positions in the circumferential direction. Comparing Figure 13(b, c, d) with Figure 13(a), it is found that the cord force with velocity will be significantly larger than the static cord force. However, as the speed increases, the maximum force on the cord does not change. On the whole, no matter whether the tire is stationary or moving, the force on the belt cord shows obvious asymmetry, and this phenomenon
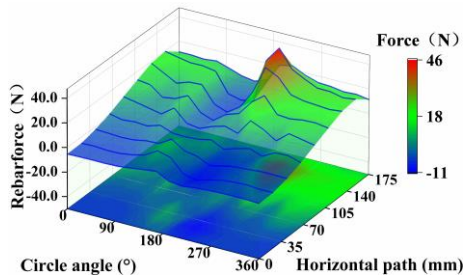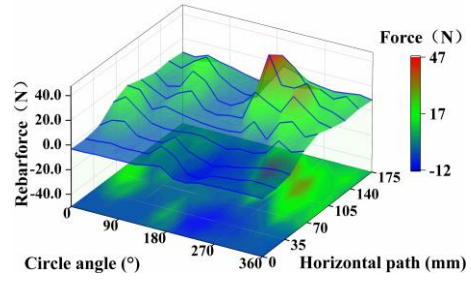
will become more obvious as the speed increases.
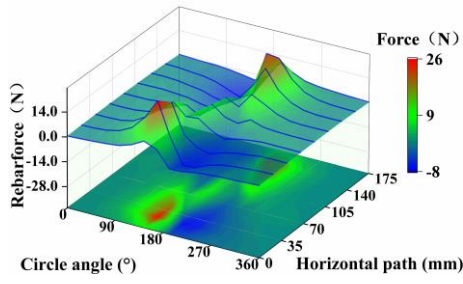
(a) 0km/h
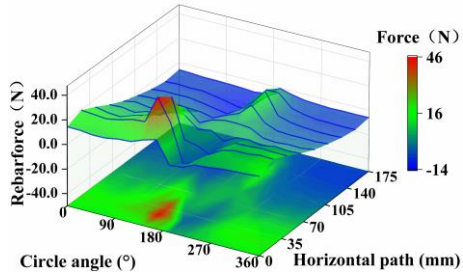
(b) 40km/h
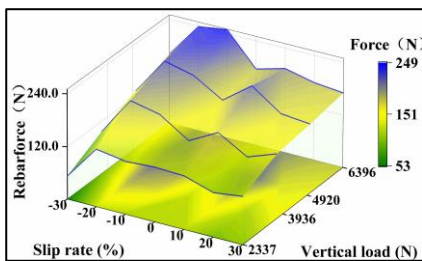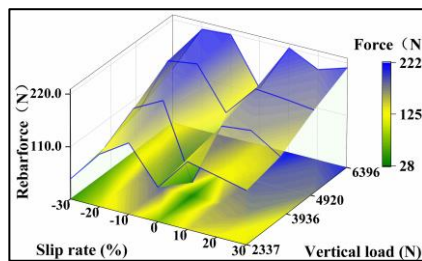

(c) 60km/h

(d) 80km/h

Figure 13   Rebarforce analysis of belt layers along the tire circumferential and axial directions at different speeds

5.2 Circumferential force analysis at the frame material reversal point

In order to study the easily damaged position of the tire frame in the longitudinal sliding process and find out the limit value of the force of each reinforcement layer. The maximum value of the Rebarforce in the circumferential direction of the fetal crown ply, the first belt ply and the first ply at different loads and speeds was analyzed. Draw the Slip rate-Vertical load-Rebarforce curve as shown in Figures 14, 15 and 16. From Figure 14, it is found that the Rebarforce of the fetal crown layer increases as the load increases. At the same time, from the comparison of the three graphs in Figure 14 (a, b, c), it is found that when the slip rate of the fetal crown layer is 0, the force on the cord is the smallest. The Rebarforce of the fetal crown layer near the slip rate of 10% and -10% will be much larger than other times. This is consistent with the slip rate corresponding to the extreme longitudinal force of the tire. This shows that there is a positive correlation between the Rebarforce on the fetal crown layer and the longitudinal force of the tire. When the speed increases from 40km/h to 80km/h, the value range of Rebarforce becomes larger, and the fluctuation becomes more severe.

(a) 40 km/h

(b) 60 km/h
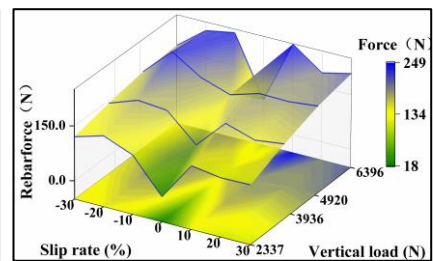
(c) 80 km/h

Figure 14   Slip rate-Vertical load-Rebarforce curves of the reverse envelope point of the fetal crown layer at different speeds

It can be seen from Figure 15 that the effect of slip   ratio on belt Rebarforce is not too prominent. This is

related to the arrangement angle of the cords of the belt layer, and a certain belt angle causes the Rebarforce to be dispersed along the circumference of the belt layer. From the stress gradient table in Figure 15 (a, b, c), it is found that the maximum stress on the belt layer at 80km/h is 49N, which is significantly larger than that at 40km/h and

60km/h. The maximum value and range of Rebarforce at 60km/h are significantly smaller than those of the other two speeds. This shows that the tire pressure and loss caused by 60km/h on the belt during the sliding process is the smallest.
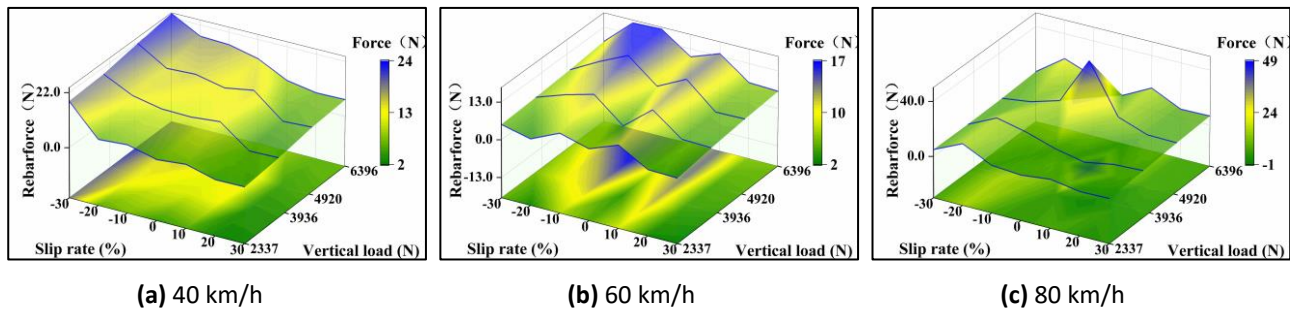

(a) 40 km/h **(b)** 60 km/h **(c)** 80 km/h

Figure 15 Slip rate-Vertical load-Rebarforce curves of the reverse envelope point of the belt layer at different speeds

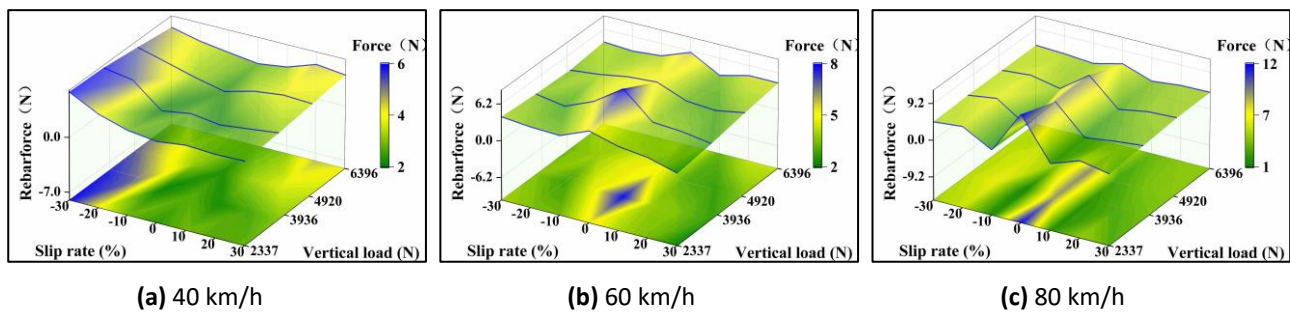

(a) 40 km/h **(b)** 60 km/h **(c)** 80 km/h

Figure 16 Slip rate-Vertical load-Rebarforce curves of the reverse envelope point of the ply layer at different speeds

The Rebarforce on the reverse wrapping point on the ply is shown in Figure 16. Analyzing Figure 16(a, b, c), it is found that as the speed increases, the maximum value of Rebarforce on the cord increases. Rebarforce volatility has also become violent as the slip rate has changed. At 0 slippage, Rebarforce becomes maximum. As the load increases, the Rebarforce on the cord does not increase significantly, but reaches a maximum value near 2337 N.

By comparing Figures 14-16, the Rebarforce on the fetal crown ply is significantly larger than that of the belt ply and the ply. Rebarforce also fluctuates more strongly with load and slip rate. The Rebarforce on the belt layer and the ply shows a decreasing trend in turn, which is related to the closer to the grounding position. With the change of velocity and slip rate, the rebarforce on each skeleton layer shows a relatively strong vibration effect. Therefore, in the tire manufacturing process, the bonding strength of the turn-up point and the tire compound should be strengthened, especially the turn-up point of the fetal crown layer with a relatively large force.

6 Conclusions

This paper firstly conducts material tests on skeleton materials such as tire compounds and cords, and determines the relevant parameters and mechanical properties. These parameters are then used to build a finite element model of the tire. The dynamic longitudinal slip test and simulation of the tire were carried out. The feasibility of the model is verified by the longitudinal force comparison of different slip rates. Then the internal skeleton structure of the tire model is analyzed. Analysis of the Rebarforce in the circumferential direction of the belt at different speeds. And the analysis of the circumferential Rebarforce extreme value on the fetal crown, belt and ply affected by load and slip rate at different speeds. Concluded as follow:

(1) The tire belt cord Rebarforce action area is consistent with the cord arrangement angle of 67° and there is asymmetry. The stress area of the belt layer is mainly concentrated in the vicinity of 180° in the circumferential direction and 35mm and 140mm in the axial direction. It is proved that the corner of the tire shoulder at the center of the ground contact will cause the concentration of the stress on the cord. With the increase of the speed, the belt cord stress will fluctuate obviously. The maximum stress did not change much and remained stable at around 46 N.

(2) The variation trend of the Rebarforce with the slip rate at the capping point is similar to the variation trend of the longitudinal force. When the slip ratio is 0, the stress on the cord is minimal. However, the maximum stress value occurs when the slip ratio is around -10% and 10%. Among them, the maximum stress values of 40km/h and 80km/h are larger, both of which are 249 N. The maximum stress value at 60km/h is a minimum of 222 N.

(3) The variation trend of the Rebarforce with the slip rate at the capping point is similar to the variation trend of the longitudinal force. When the slip ratio is 0, the stress on the cord is minimal. However, the maximum stress value occurs when the slip ratio is around -10% and 10%. Among them, the maximum stress values of 40km/h and 80km/h are larger, both of which are 249 N. The maximum stress value at 60km/h is a minimum of 222 N.

(4) The fluctuation phenomenon of Rebarforce with slip rate at the reversal point of the ply layer is obviously more moderate than that of the fetal crown layer and the belt layer. The Rebarforce on the fetal crown and belt wrapping points increases with the increase of the load. The Rebarforce of the ply wrapping point is relatively gentle, but has an extreme value at 2337 N. It shows that the degree of damage to the ply is far less than that of the fetal crown layer and the belt layer.

7　Declaration

Availability of data and materials

The datasets supporting the conclusions of this article are included within the article.

Authors' contributions

The author' contributions are as follows: Peng-Fei Sun was in charge of the whole trial; Lu-Wen Chen wrote the manuscript; Lu-Wen Chen assisted with sampling and laboratory analyses.

Competing interests

The authors declare no competing financial interests.

Consent for publication

Not applicable

Ethics approval and consent to participate

Not applicable

References

[1] Wei Yintao, Shen Xiaoliang. Tire steady-state kinematics and six component force prediction I: Theory and method. *Journal of mechanical engineering*, 2012, 48(15): 65-74. (in Chinese).

[2] Li Li, Liu Weidong, Xiao Peiguang, Dang Dong. Analysis of tire grounding characteristics and static stiffness based on ABAQUS modeling. *Special Rubber Products*, 2016, 37(04): 38-43.

[3] Ge Shuqing, Wang Baoliang. Analysis and Test Verification of Tire Grounding Characteristics. *Mechanical Design and Manufacturing*, 2014, (07): 233-235.

[4] Chen Wenyuan. Research on tire grounding impression based on finite element analysis. *Rubber and Plastic Technology and Equipment*, 2018, 44(15): 49-53.

[5] Shoop S, Darnell I, Kestler K. Analysis of tire models for rolling on a deformable substrate. *Tireland Science and Technology*, 2002, 30 (3): 180-197.

[6] Jenog KM. Prediction of burst pressure of a radial truck tire using fnite element analysis. *World J Eng Technol*, 2016, 4(2): 228–237.

[7] Li Quantong, Wang Xiangyu, Zhang Bangji, Li Liang. Research on Tire Longitudinal-vertical Coupling State Observation and Slip Ratio Control under Bumpy Road. *Journal of Mechanical Engineering*, 2021, 57(12): 62.

[8] Haichao Zhou, Huiyun Li, Jian Yang, Qingyun Chen, Guolin Wang, Tong Han, Jieyu Ren, Te Ma. A Strain-Based Method to Estimate Longitudinal Force for Intelligent Tires by Using a Physics-Based Model. *Journal of Mechanical Engineering*, 2021, 67(4): 153-166.

[9] Zhou F, Guo K, Li Y, Dang X. Mechanical Properties of Tire during Static Steering Based on Offset Steering Shaft. *Transactions of the Chinese Society for Agricultural Machinery*, 2021, 52(1): 385-392,417.

[10] Tian L, Wang D, Su P, Wei Q. A study on the viscoelastic behaviors of tire cords using dynamic mechanical analysis. *Journal*

of Engineered Fibers and Fabrics, 2020, 15(81).

[11] Sun P, Huang H, Zhou S. Experiment and Analysis of Cord Stress on High-Speed Radial Tire Standing Waves. *Shock & Vibration*, 2019, 2019(3): 1-9.

[12] Zhou S T, Du M, Sun P F, et al. Experimental and theoretical analysis of high-speed radial tire standing waves. *Journal of the Brazilian Society of Mechanical Sciences and Engineering*, 2020, 42(4).

Biographical notes

Shui-Ting Zhou, born in 1970, is currently an professor at *Xiamen University of Technology, China.*
E-mail: zhoushuiting@xmut.edu.cn

Lu-Wen Chen, born in 1995, is currently a master candidate at *Key Laboratory of Advanced Design and Manufacturing for Passenger Cars, Xiamen University of Technology, China.* His research direction is tire dynamics
Tel: +86-17824240730; E-mail: 1210271096@qq.com

Peng-Fei Sun, born in 1986, is currently an professor at *Xiamen University of Technology, China.*
E-mail: sunpengfei@xmut.edu.cn

Junling Meng, born in 1999, is currently a master candidate at Key Laboratory of Advanced Design and Manufacturing for Passenger Cars, Xiamen University of Technology, China.
E-mail: 2655887078@qq.com

Chao Qian, born in 1993, is currently a master candidate at *Key Laboratory of Advanced Design and Manufacturing for Passenger Cars, Xiamen University of Technology, China.*
E-mail: 382163882@qq.com

Xin Sun, born in 1997, is currently a master candidate at *Key Laboratory of Advanced Design and Manufacturing for Passenger Cars, Xiamen University of Technology, China.*
E-mail: 975192239@qq.com

Appendix

Appendix and supplement both mean material added at the end of a book. An appendix gives useful additional information, but even without it the rest of the book is complete.